Journal of Organometallic Chemistry 980–981 (2022) 122509

Contents lists available at ScienceDirect

Journal of Organometallic Chemistry

journal homepage: www.elsevier.com/locate/jorganchem

Double-decker lutetium and europium phthalocyanine composites with reduced graphene oxide as supercapacitor electrode materials

Ebru Yabaş[a,*], Emre Biçer[b], Mete Batuhan Durukan[c,d], Deniz Keskin[c,d], Husnu Emrah Unalan[c,d,*]

[a] Sivas Cumhuriyet University, Advanced Technology Application and Research Center, 58140, Sivas, Turkey
[b] Sivas University of Science and Technology, Faculty of Engineering and Natural Sciences, 58140, Sivas, Turkey
[c] Department of Metallurgical and Materials Engineering, Middle East Technical University (METU), 06800 Ankara, Turkey
[d] Energy Storage Materials and Devices Research Center (ENDAM), Middle East Technical University (METU),06800 Ankara, Turkey

ARTICLE INFO

Article history:
Received 23 May 2022
Revised 27 August 2022
Accepted 2 September 2022
Available online 7 September 2022

Keywords:
Double-decker phthalocyanines
Supercapacitors
Nanocomposites
Lutetium
Europium

ABSTRACT

Double-decker phthalocyanines were synthesized by a classical method with phthalonitrile and lanthanide metal salts, europium and lutetium acetate. Non-covalent double-decker phthalocyanine-reduced graphene oxide (MPc_2/rGO) composites were then prepared by simple sonication method. All the phthalocyanines were peripheral tetrasubstituted 5-(3-pyridyl)-1,3,4-oxadiazole. Following spectroscopic and morphological characterisation, fabricated composites were subjected to detailed electrochemical analysis. $EuPc_2$/rGO and $LuPc_2$/rGO composite electrodes showed specific capacitance values of 115 F/g and 86 F/g, respectively. Coulombic efficiency values for those materials were determined as 85% and 74%, respectively, at a significant current density of 5 A/g. Following 5000 cycles, $EuPc_2$/rGO and $LuPc_2$/rGO electrodes retained 93% and 99% of their initial capacitance, respectively. These results demonstrated the significant electrochemical performance of double-decker phthalocyanines and can be certainly extended to other metal salts or other composite formers with double-decker phthalocyanines.

1. Introduction

Phthalocyanines are highly promising for decades with typical uses in applications such as organic semiconductors [1], gas sensors [2], photovoltaic cells [3], catalysis [4], and photoluminescence [5]. Phthalocyanines possess 18 π-electrons delocalized around four isoindole units with active nitrogen sites that involve in redox reactions in many applications [6]. Because of their high coordination numbers and large ion radii, lanthanides can form double-decker phthalocyanines together with phthalocyanines. These compounds, which have strong π-π interaction between macrocycles, have superior semiconductor nature compared to their monomeric counterparts. On the other hand, double-decker phthalocyanines, also known as stable radicals, have interesting electrical and electrochemical properties and show higher conductivity and carrier mobility than monomeric phthalocyanines. Double-decker phthalocyanines, and especially lutetium derivatives, have been the subject of extensive research regarding their electrochemical and electrochromic properties, intrinsic semiconductivity, and third-order optical nonlinearity. Their various properties appear to be susceptible to ring substituents and central metal, but many details are still poorly understood. Studies on this type of compound are ongoing. It is seen that conjugated π systems, which play an important role in applications in such structures, are kept close especially by metal ions, and interactions between rings provide many features in applications. On the other hand, phthalocyanines are highly compatible with carbon-based materials such as graphene, carbon nanotubes (CNTs) through surface coordination via π-π interactions. Composites of phthalocyanines and carbonaceous materials are utilized as electrodes in energy storage systems and revealed promising electrochemical response and prominent charge transfer efficiency [7,8].

As an energy storage system, supercapacitors have high energy density, high charge/discharge rate and long cycle life [8]. The electrochemical performance of supercapacitor is provided in two different ways. First one is a non-Faradaic process, where no charge transfer occurs at the electrode-electrolyte interface, also called as electrochemical double layer capacitance (EDLC). The second one is called pseudo-capacitance, where a reversible redox reaction takes place between electrode active species and the electrolyte [9]. Significant efforts have been spent on the use of transition metal oxides as electrode active materials in supercapacitors, likewise nitrides and sulfides [10]. Recently, the use of metal phthalocyanines

* Corresponding authors.
E-mail addresses: eyabas@cumhuriyet.edu.tr (E. Yabaş), unalan@metu.edu.tr (H.E. Unalan).

https://doi.org/10.1016/j.jorganchem.2022.122509
0022-328X/

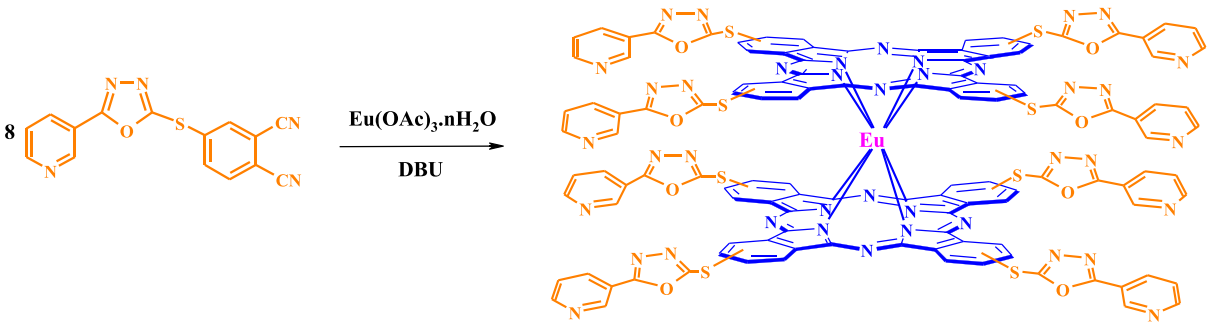

Fig. 1. A schematic showing the synthesis route for $EuPc_2$.

(MPcs) in charge storage applications was demonstrated and became a popular issue, namely such as NiPc [11], CuPc [8], FePc, and CoPc [7,12–15]. Madhuri and John reported a specific capacitance of 223 F/g at a current density of 1 A/g from NiPc fiber/rGO hybrids. A capacity retention of 88% following 1100 cycles was also obtained [11]. Another FePc-NH_2/rGO hybrid material was exposed by Otyepka and co-workers demonstrating a gravimetric capacity of 960 F/g at 1 A/g. Unlike this study, FePc-NH_2 was anchored on the surface of graphene by covalent bond. This feature gave covalently-bonded phthalocyanine durability, thus showing a high cycle life without capacity fading [19].

MPcs, showed excellent electron transport ability by the interaction of aromatic phthalocyanine ring and central metal atom in the inner ring [16]. As a consequence, unsubstituted MPcs have less solubility in aqueous medium than the substituted MPcs [17]. This is a limitation for substituted MPcs to be used in energy storage devices, especially in supercapacitors utilizing aqueous electrolytes. However, since the electrochemical properties are vastly dependent on the interface of the electrodes, formation of composites with MPcs provide a broad range of options to control the structure and morphology. This feature allowed these materials to perform as a prominent supercapacitive material in terms of capacity, charge/discharge rate and cycle life compared with the traditional metal oxide compounds. The use of conductive carbon materials as additives to the electrochemical matrix offer a solution to low conductivity MPcs. Among these carbon materials, graphene offers the best performance by providing high surface area, flexible chemical tunability, high electrical and thermal conductivity [18]. Graphene functionalized with MPc seems to be promising supercapacitor material within higher mechanochemical properties, specific surface area and better electrical properties [19].

Based on the above considerations, we have investigated the electrochemical performance of π-π stacked double-decker phthalocyanine and reduced graphene oxide (rGO) nanocomposites. For this purpose we have utilized double decker Lutetium and Europium phthalocyanines ($LuPc_2$ and $EuPc_2$), which, to the best of our knowledge, was not demonstrated in literature in composite form with rGO.

2. Experimental

2.1. Materials and instruments

All solvents were dried by molecular sieves or proper methods, and these solvents were used under nitrogen atmosphere in the reactions [20]. 4[(5-(3-pyridyl)-1,3,4-oxadiazole)-

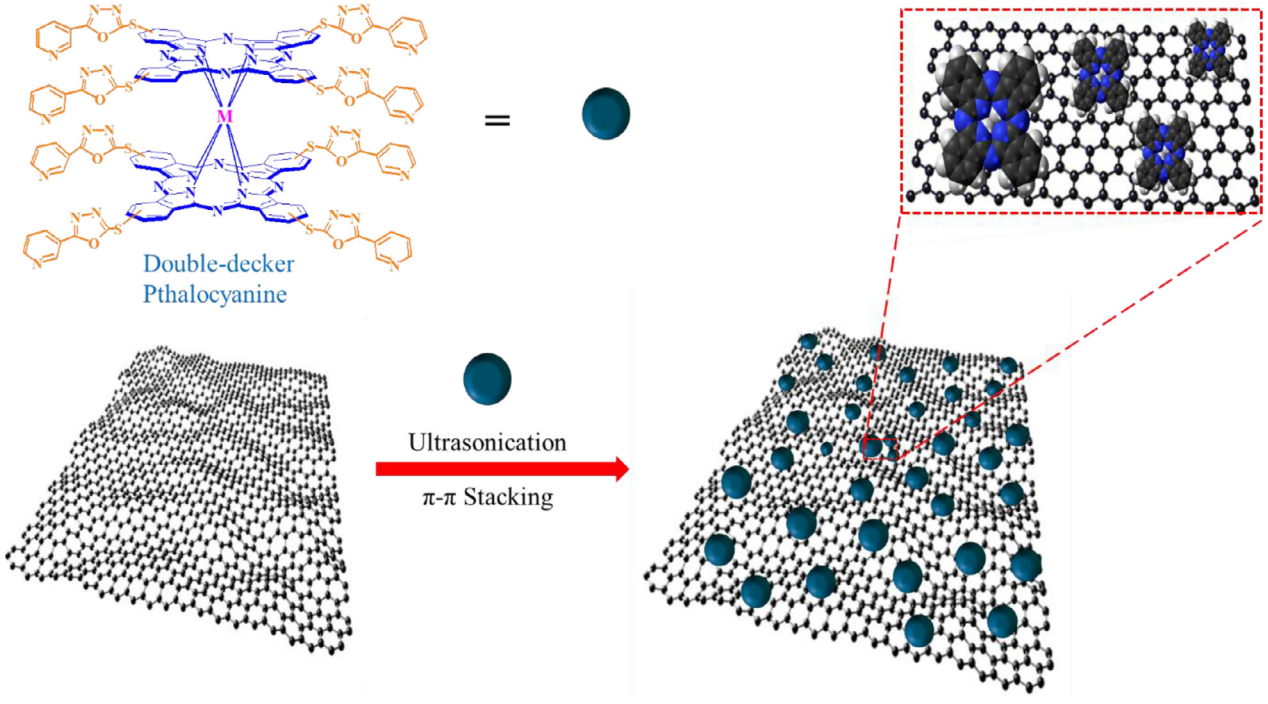

Fig. 2. A schematic showing the preparation method of MPc_2/rGO composites.

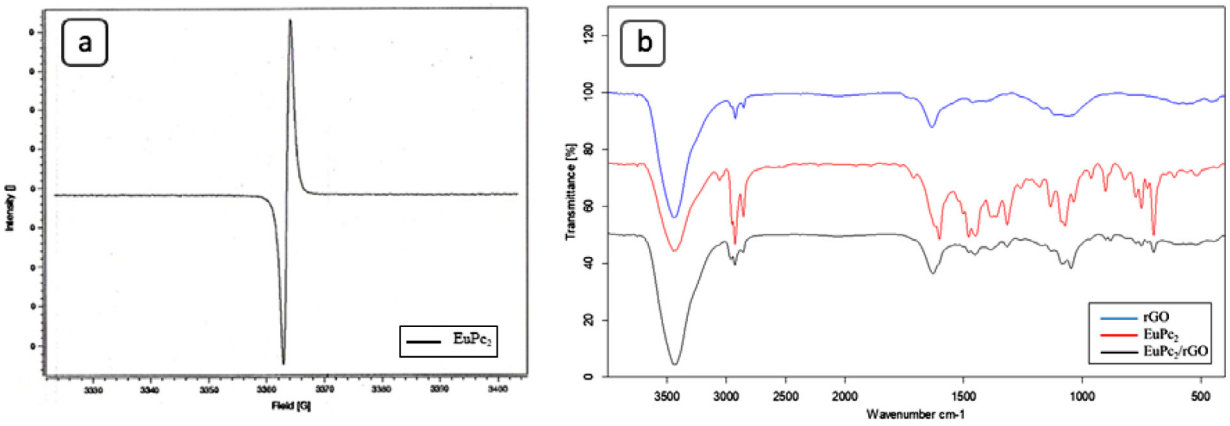

Fig. 3. (a) X-band ESR spectra of double-decker $EuPc_2$ and (b) FT-IR spectra of rGO, $EuPc_2$, $EuPc_2$/rGO.

2-thio]phthalonitrile and bis[tetra-2,9,16,23-{(5-(3-pyridyl)-1,3,4-oxadiazole)-2-thio} phthalocyaninato]lutetium(III) were prepared according to the literature [21]. All chemicals and rGO were purchased from Sigma-Aldrich and Merck. Sonics VCX-750 Vibra Cell was used for the sonication process. FT-IR analysis was conducted with ATR by Bruker Tensor II FT-IR spectrophotometer. UV-Vis spectra were recorded in the Shimadzu UV-1800 UV-Vis spectrophotometer. ^{1}H-NMR spectra were taken in JEOL Resonance ECZ400S 400 MHz spectrometer. SEM analysis was conducted using a TESCAN® MIRA3 XMU (Brno, Czechia) brand scanning electron microscope.

2.2. Synthesis of compounds

2.2.1. Bis[tetra-2,9,16,23-{(5-(3-pyridyl)-1,3,4-oxadiazole)-2-thio}phthalocyaninato]europium(III)

A mixture of 4-[(5-(3-pyridyl)-1,3,4-oxadiazol)-2-thio]phthalonitrile (100.0 mg, 0.3 mmol), $Eu(OAc)_3.nH_2O$ (13.0 mg, 0.04 mmol), 1,8-Diazabicyclo[5.4.0]undec-7-ene (DBU) and 1-hexanol (0.3 mL) was heated at 300°C for 45 min. in a pressure-resistant sealed glass tube under nitrogen atmosphere. After the reaction was terminated, the mixture was cooled and the organic phase was precipitated with methyl alcohol (MeOH), filtered off. The crude product was washed with MeOH (3 × 5 mL) and acetone (3 × 5 mL), respectively. The green product dried under vacuum. The compound was dissolved in N,N-dimethyl formamide (DMF) and impurities were filtered off. The dark green solution was precipitated by the addition of MeOH, filtered off, and dried under vacuum. The dark green compound was soluble in tetrahydrofuran (THF), DMF and dimethyl sulfoxide (DMSO). Yield 38.0 mg (36%). Mp: >300°C. ^{1}H-NMR for reduced form of 2 (400 MHz, DMSO-d_6 in the presence of hydrazine hydrate (1% v/v)): δ = 9.2-8.9 (br, 24H, Pc Ar-H); 8.1-7.0 (br, 32H, Pyridyl Ar-H). UV-vis (DMSO) λ_{max}/nm (log ε, dm^3 mol^{-1} cm^{-1}) 700 (5.40), 621 (4.63), 472 (4.37), 361 (4.83). FT-IR (ATR) υ (cm^{-1}) 3057, 2926, 1602, 1479, 1316, 751. Anal. Calc. for $C_{120}H_{56}N_{38}O_8S_8Eu$: C 55.54; H 2.18; N 20.51%, found: C 54.99; H 2.05; N 19.92%. MALDI-TOF MS m/z: 2596 $[M+H]^+$

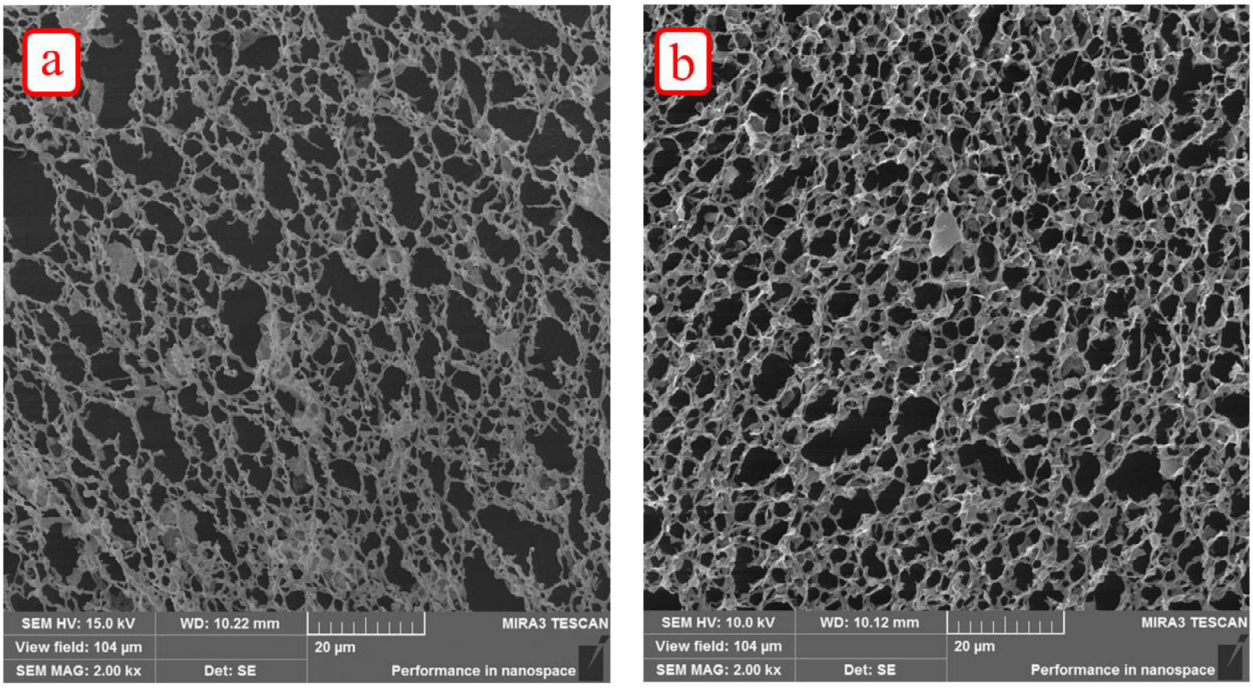

Fig. 4. SEM images of (a) $LuPc_2$/rGO (1 µg/mL / 1 µg/mL) and (b) $EuPc_2$/rGO (1 µg/mL / 1 µg/mL) composites.

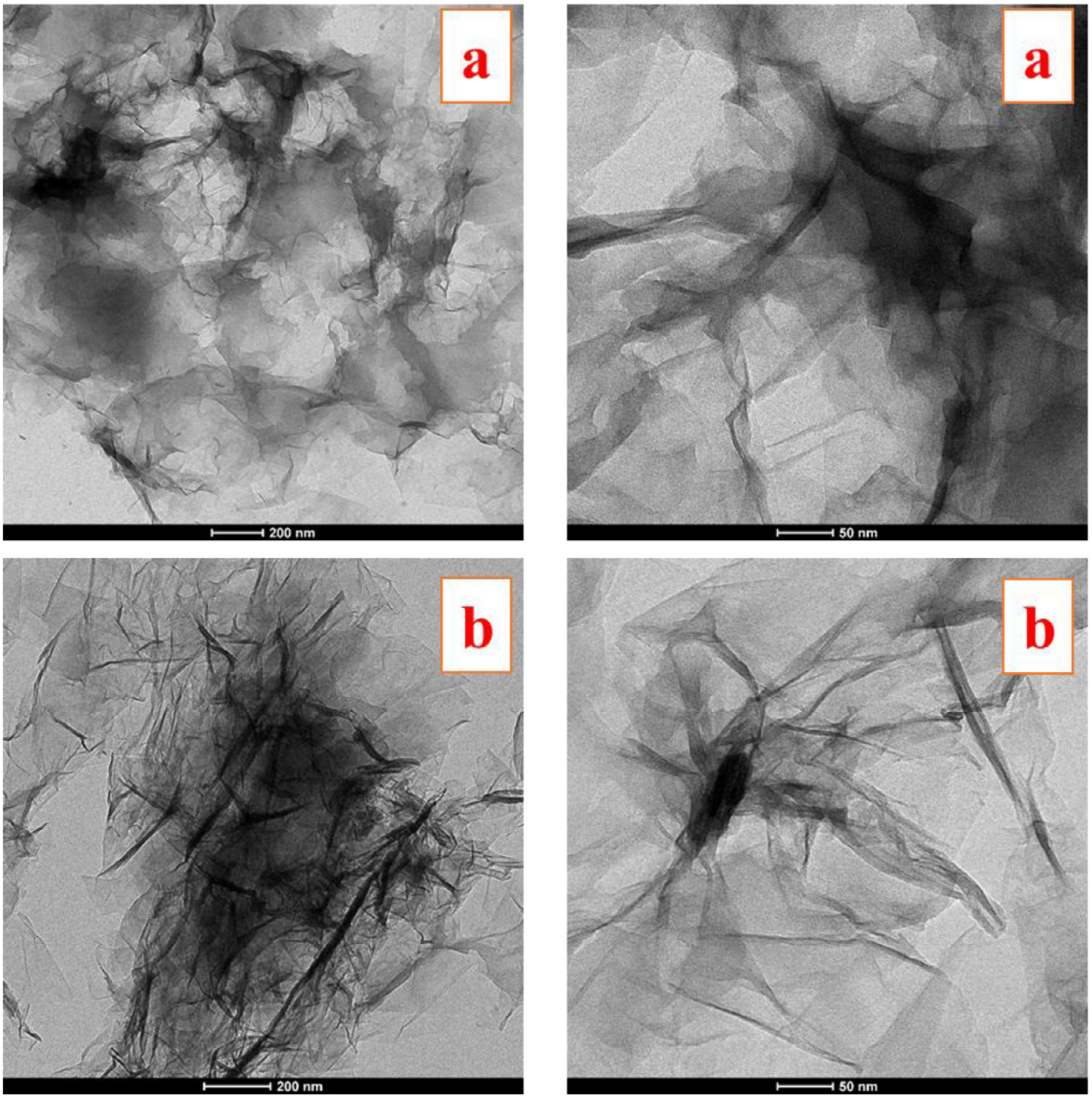

Fig. 5. TEM images of (a) $LuPc_2$/rGO (1 μg/mL / 1 μg/mL) and (b) $EuPc_2$/rGO (1 μg/mL / 1 μg/mL) composites.

2.2.2. $LuPc_2$/rGO and $EuPc_2$/rGO composites

rGO solutions (0.00001 μg/mL; 0.0001 μg/mL; 0.001 μg/mL; 0.01 μg/mL; 0.1 μg/mL; 1 μg/mL) were prepared using DMSO as solvent by sonication. The solution of 1 μg/mL of $LuPc_2$ or $EuPc_2$ in DMSO (5 mL) was added to different concentrations of rGO solutions (5 mL), respectively. The prepared solutions were sonicated for 15 min.

2.3. Electrochemical analysis

2.3.1. Preparation of supercapacitor electrodes

Materials were obtained in powder form and mixed with carbon black and polyvinylidene fluoride (PVDF) solution (5 wt.% in NMP) in the ratio of 80:10:10, respectively. Obtained slurry was coated onto precleaned nickel (Ni) foams via dipping at least 5 times and vacuum dried at elevated temperature. Following dip-coating, samples were compressed via a hot roller press machine and weighed to determine the amount of deposited material. Active mass for $EuPc_2$ and $LuPc_2$ were approximately 2.5 and 3.2 mg, respectively.

2.3.2. Electrochemical setup

Electrochemical analysis was conducted using a Biologic VMP3 galvanostat/potentiostat system. A 3-electrode setup was used, where $EuPc_2$/rGO and $LuPc_2$/rGO coated Ni foams, platinum (Pt) foil and saturated calomel electrode (SCE) in saturated potassium chloride (KCl) were used as working electrode, counter electrode, and reference electrode, respectively. 1 M potassium hydroxide (KOH) was used as the electrolyte. Cyclic voltammetry (CV), galvanostatic charge-discharge (GCD) and potentiostatic impedance spectroscopy (PEIS) were utilized to obtain electrochemical data.

3. Results and discussion

In the present study, bis[tetra-2,9,16,23-{(5-(3-pyridyl)-1,3,4-oxadiazole)-2-thio} phthalocyaninato]lutetium(III) ($LuPc_2$) was prepared according to the literature [21]. Similarly, bis[tetra-2,9,16,23-{(5-(3-pyridyl)-1,3,4-oxadiazole)-2-thio}phthalocyaninato] europium(III) ($EuPc_2$) was synthesized by cyclotetramerization of phthalonitrile and europium acetate in basic medium (Fig. 1). $LuPc_2$ ve $EuPc_2$ have synthesized with the same conditions with

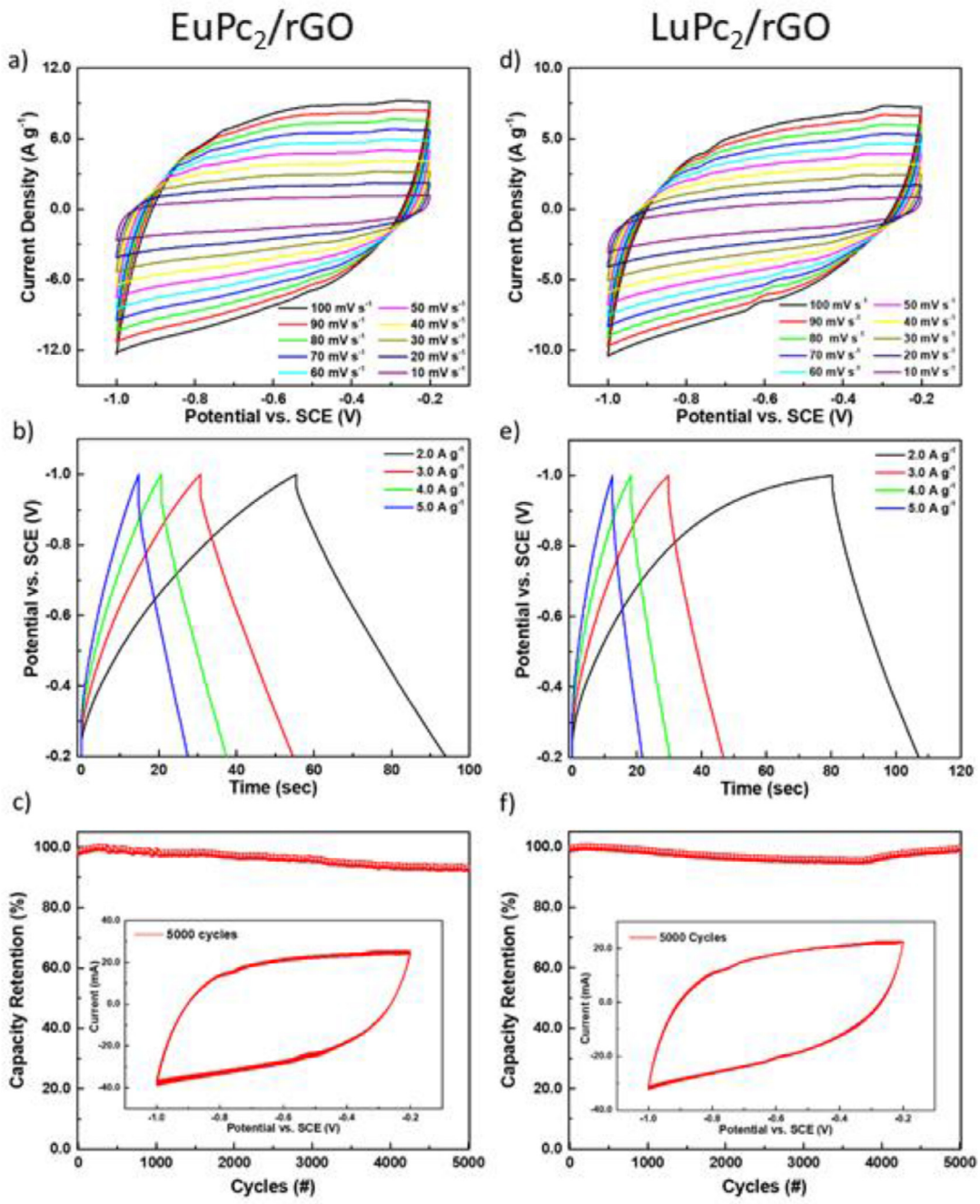

Fig. 6. (a,d) Cyclic voltammogram, (b,e) galvanostatic charge discharge and (c,f) cycling stability graphs of $EuPc_2$/rGO and $LuPc_2$/rGO, respectively. Inset figures in (c) and (f) show the voltammograms of 5000th cycles.

29% and 36% yields with 90 min. and 45 min. $LuPc_2$ and $EuPc_2$ were obtained with 29% and 36% yields, respectively, after 90 min. and 45 min. reaction times under similar conditions. It can be speculated that these yield and reaction time differences are due to the ion radius of Eu is larger than of Lu and that $EuPc_2$ formation is less affected by the steric factors that occur with the addition of the second Pc ligand.

Composites were then prepared by sonication of reduced graphene oxide (rGO) and double-decker phthalocyanines (Fig. 2).

The ESR spectrum of $EuPc_2$ at room temperature presented a strong signal at g: 2.0074 with a bandwidth of 5.86 G (Fig. 3a). This result showed the formation and the paramagnetic nature of europium-centered double-decker phthalocyanine [21]. In the FT-IR spectrum of $EuPc_2$, the characteristic vibrational band of the C≡N group, which appeared at 2241 cm^{-1} of the phthalonitrile derivative [21], disappeared after double-decker phthalocyanine conversion (Fig. 3b). The typical IR marker band of the $Pc^{\cdot-}$ π-radical anion for double-decker $EuPc_2$ is showed a band at 1316 cm^{-1} [22]. These results confirmed the formation of double-decker phthalocyanine structure as a result of the cyclotetramerization reaction of phthalonitrile. The UV-Vis spectra of $EuPc_2$ showed a peak at 700 nm for Q-band absorption and at 361 nm for B-band absorption. The characteristic absorption peak for the radical phthalocyanine anion in double-decker phthalocyanines appeared at 472 nm for double-decker europium phthalocyanine [22,23]. The ^{1}H-NMR spectrum in the presence of hydrazine hydrate (1%, v/v) of $EuPc_2$ showed aromatic protons between 9.2 and 7.0 ppm [21]. Elemental analysis results of $EuPc_2$ were also in line with the structure.

A sonication process was used to prepare non-covalent rGO composites of double-decker lutetium and europium phthalocyanines via $\pi-\pi$ interaction. Various concentrations of MPc_2/rGO (MPc_2: 1 μg/mL; rGO: 0.00001 μg/mL; 0.0001 μg/mL; 0.001 μg/mL; 0.01 μg/mL; 0.1 μg/mL; 1 μg/mL) were prepared in DMSO to provide the interaction between the double-decker phthaocyanines and rGO. Following the formation of $LuPc_2$/rGO and $EuPc_2$/rGO composites, a redshift was observed in UV-Vis spectra. This shift accounts for the $\pi-\pi$ interaction illustrating the flattening of the curves by increasing the amount of rGO [24,25]. Fig. 3b compares the FT-IR spectrum of the rGO, $LuPc_2$ and $LuPc_2$/rGO composites. In the FT-IR spectrum of rGO, bands of -OH stretching, skeletal vibrations of unoxidized graphitic areas, OH deformations of C-OH groups and stretching vibrations of CO groups were observed as broad bands. Following the interaction of rGO with $LuPc_2$ or $EuPc_2$, the intensity of the bands associated with their oxygen functionalities were found to decrease. As a result of the $LuPc_2$/rGO and $EuPc_2$/rGO composite formation, a general shift in the FT-IR bands were observed. This was attributed to an increase in the electron density due to the energy transfer between rGO and double-decker phthalocyanine compounds [26]. Overall, FT-IR spectra showed the formation of composites of rGO and double-decker phthalocyanine [27].

SEM images of $LuPc_2$/rGO and $EuPc_2$/rGO composites are provided in Fig. 4. Partial agglomeration of rGO with $LuPc_2$ and $EuPc_2$ in DMSO solution can be observed in Fig. 4a and 4b, respectively. Formation of a continuous and porous rGO network enhanced the interaction between rGO and double-decker phthalocyanines in the composites. It is also observed from the SEM images that the average pore size of the $EuPc_2$/rGO composite was lower than that of $LuPc_2$/rGO composite. In this case, it can be said that $EuPc_2$/rGO composite has better π-π stacking bonds than $LuPc_2$/rGO. This structure can improve the charge transfer and decrease the charge transfer resistance in electrochemical systems. In addition, TEM images of $LuPc_2$/rGO and $EuPc_2$/rGO composites were taken to further reveal the distribution of $LuPc_2$ and $EuPc_2$ on rGO. Fig. 5 shows TEM images of $LuPc_2$/rGO and $EuPc_2$/rGO composites at different magnifications. In the TEM images, as in the SEM images, the interaction in the $EuPc_2$/rGO composite seems to be higher than in the $LuPc_2$/rGO composite.

Electrochemical characteristics of the fabricated $EuPc_2$/rGO and $LuPc_2$/rGO composites are provided in Fig. 6. Typical rectangular cyclic voltammogramms were obtained for both composites without any evident redox peaks (Fig. 6a and 6d) at scan rates ranging from 10 to 100 mV/s. These rectangular shapes indicated highly reversible, ideal pseudocapacitive behavior [28]. This ideal pseudocapacitive behavior can also be observed from GCD plots provided in Fig. 6b and 6e. For $EuPc_2$/rGO composites, GCD plots had an almost symmetrical shape, further proving the ideal-like behavior (Fig. 6b). Coulombic efficiency was calculated as 85% at a current density of 5 A/g, which decreased to 71% at 2 A/g. This showed that $EuPc_2$/rGO composites are highly promising for high-rate energy storage applications. On the other hand, $LuPc_2$/rGO composites showed lower efficiencies compared to $EuPc_2$/rGO counterparts. Coulombic efficiencies of 74% to 34% were obtained at current densities of 5 A/g and 2 A/g, respectively. This could be related with higher leakage currents in $LuPc_2$/rGO composites when compared to $EuPc_2$/rGO, yet does not hinder its high-rate capability and related applications.

Lastly, cyclic stability tests were conducted for both composites at a scan rate of 100 mV/s, results of which are provided in Fig. 6c and 6f. After 5000 cycles, $EuPc_2$/rGO composites showed significant stability and retained 93% of their initial capacitance (Fig. 6c). This can be attributed both to ideal pseudocapacitive behavior of Eu and also the addition of rGO [28]. For the case of $LuPc_2$/rGO, capacitance retention was dropped to 95%, around 3800 cycles, yet reached up to 99% at the end of 5000 cycles (Fig. 6f). Inset of Fig. 6f also proves that there is no apparent degradation in the performance of $LuPc_2$/rGO. The reason for this increase remains elusive and may need further analysis on $LuPc_2$/rGO composites.

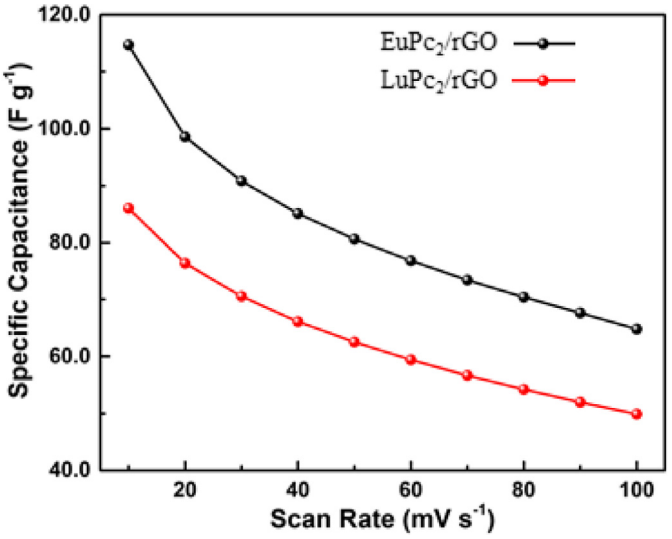

Fig. 7. Specific capacitances of $EuPc_2$/rGO and $LuPc_2$/rGO composites at varying scan rates.

Specific capacitances (C_{sp}) of the $EuPc_2$/rGO and $LuPc_2$/rGO composites were calculated using the equation;

$$C_{sp} = \frac{\int_{Ef}^{Ei} I dE}{2\ m\ v\ \Delta E} \quad (1)$$

,where I is the instantaneous current (mA), m is the mass of active material (g), v is the scan rate (mV s^{-1}), and ΔE is the potential range (V). Specific capacitance values were calculated from Fig. 7a and d for $EuPc_2$/rGO and $LuPc_2$/rGO, respectively, and the results are provided in Fig. 7. $EuPc_2$/rGO composite yielded a maximum capacitance of 114.7 F/g at a scan rate of 10 mV s^{-1}. An almost linear drop-down was observed with increased scan rates. On the other hand, $LuPc_2$/rGO composites showed a maximum capacitance of 86.0 F/g at a scan rate of 10 mV s^{-1}. Both composites had a promising supercapacitive behavior, which scaled up linearly starting from 30 mV/s up to 100 mV/s, indicating significant rate capability. Breaking from the linearity below 30 mV/s can be explained by the longer diffusion times of the ions from the pores of the phthalocyanine structures.

For the sake of clarity, CV and GCD results are compared and provided in Fig. 8a and 8b, respectively. Better specific capacitance of $EuPc_2$/rGO composite with respect to $LuPc_2$/rGO counterpart can be observed clearly in Fig. 8a. CV of the bare Ni foam is also provided in Fig. 8a, with no significant contribution to the capacitive properties compared to the fabricated composites. Better kinetics for $EuPc_2$/rGO composite can be observed in the GCD results provided in Fig. 8b, where the charge-discharge curves have higher symmetry than that of $LuPc_2$/rGO.

PEIS analysis was also conducted to further analyze the electrochemical behavior of fabricated $EuPc_2$/rGO and $LuPc_2$/rGO composites. Nyquist plots are provided in Fig. 8c. A frequency range of 200 kHz to 20 mHz with sinusoidal amplitude of 10 mV at open circuit voltage was used to obtain these plots. Equivalent circuit model and respective plots of fittings for $EuPc_2$ and $LuPc_2$ were given in the Fig. 8c, respectively. Very small series resistances of as low as 2.34 ohms and 1.93 ohms for $EuPc_2$/rGO and $LuPc_2$/rGO electrodes, respectively, were observed. Very small semicircles in both composites was indicative of the presence of very small charge transfer resistances, which supported the reversible behavior of both

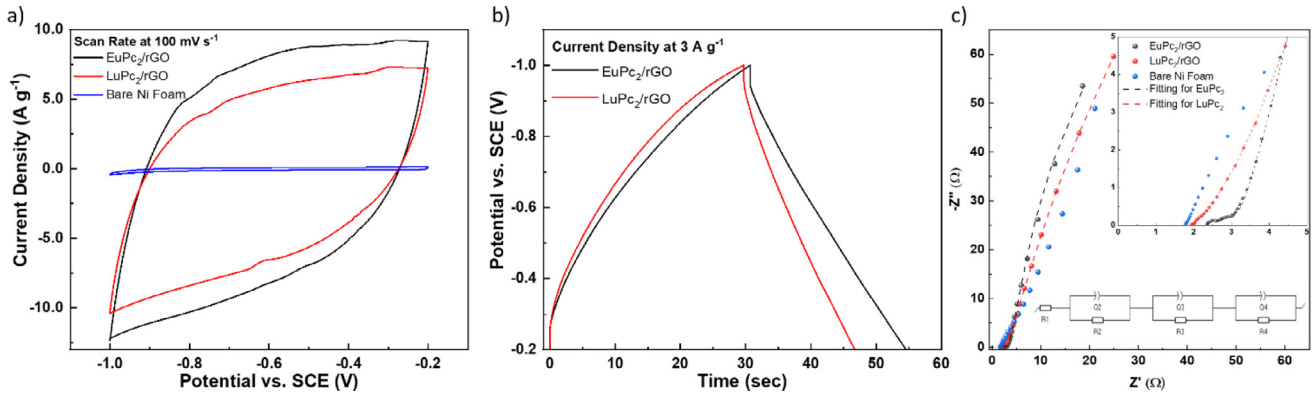

Fig. 8. (a) CV, (b) GCD and (c) PEIS comparisons of fabricated $EuPc_2$/rGO and $LuPc_2$/rGO composites.

$EuPc_2$/rGO and $LuPc_2$/rGO especially at higher charge-discharge rates. An angle that is higher than 45° in the low frequency region, is an indication of a complex storage behavior that is denoted with constant phase element (CPE) in the equivalent circuit, which is denoted as Q in the inset model. CPE can be written as

$$Z_{CPE} = \frac{1}{Q(i\omega)^n} \quad (2)$$

,where i is the imaginary part of the system, ω is the angular frequency ($\omega = 2\pi f$) of the impedance spectra, Q is the characteristic value of capacitive behavior ($F.s^{n-1}$) and n is the dimensionless CPE exponent [29,30]. Higher angle of $EuPc_2$/rGO compared to $LuPc_2$/rGO in low frequency range can also be correlated to the better kinetics and reversibility of $EuPc_2$/rGO composites. Here, n value determines the ideality. If $n = 1$, CPE behaves as an ideal capacitor; while for $n = 0$, it behaves as a resistive component. Likewise, $n = 0.5$ is the case of Warburg impedance, in which the system is controlled by diffusion especially in the case of slow Li^+ intercalation in battery electrodes [31]. Thus, it can be said that lower CPE exponent leads to non-ideal capacitive behavior [30]. Q_2 and Q_3 values are related with the nickel foam substrate and electrode/electrolyte interface, respectively. With the model provided as an inset in Fig. 7c, fitted impedance spectra yields CPE exponents (from Q_4) of 0.984 and 0.814 for $EuPc_2$/rGO and $LuPc_2$/rGO, respectively. This could be an explanation of the better capacitance value and coulombic efficiency of $EuPc_2$/rGO compared to $LuPc_2$/rGO. Ultimately, both double-decker phthalocyanines showed very promising results and kinetics to be utilized as supercapacitor electrodes.

4. Conclusions

In this study, two different double-decker phthalocyanines were prepared by metal incorporation with europium and lutetium. Both $LuPc_2$ and $EuPc_2$ were double-decker phthalocyanines gave peripheral tetrasubstituted oxadiazale structure. These phthalocyanines were incorporated with rGO in a simple way by sonication method. $EuPc_2$/rGO and $LuPc_2$/rGO composites demonstrated a good performance in supercapacitor as an active material in aqueous KOH media. $EuPc_2$/rGO showed a coulombic efficiency of 85% at the current density of 5 A/g while $LuPc_2$/rGO only presented 74%. $EuPc_2$/rGO maintained 93% of its initial capacity at a scan rate of 100 mV/s after 5000 cycles, whilst $LuPc_2$/rGO maintained 95% at 3800 cycles and then increased to 99% after 5000 cycles. Specific capacitance for $EuPc_2$/rGO and $LuPc_2$/rGO were calculated as 115 F/g, while $LuPc_2$/rGO was found to be 86 F/g. Encouraging capacitive behaviour was observed from both $EuPc_2$/rGO and $LuPc_2$/rGO active materials. Therefore, these materials can be promising candidates for positive electrodes in supercapacitors.

Declaration of Competing Interest

The authors declare that they have no known competing financial interests or personal relationships that could have appeared to influence the work reported in this paper.

Data availability

No data was used for the research described in the article.

Acknowledgments

In this study, the laboratory facilities of the Advanced Technology Application and Research Center of Sivas Cumhuriyet University (CÜTAM) were used.

References

[1] O.A. Melville, B.H. Lessard, T.P. Bender, Phthalocyanine-based organic thin-film transistors: a review of recent advances, ACS Appl. Mater. Interfaces 7 (2015) 13105.
[2] F.I. Bohrer, C.N. Colesniuc, J. Park, M.E. Ruidiaz, I.K. Schuller, A.C. Kummel, W.C. Trogler, Comparative gas sensing in cobalt, nickel, copper, zinc, and metal-free phthalocyanine chemiresistors, J. Am. Chem. Soc. 131 (2009) 478.
[3] M. Urbani, M.E. Ragoussi, M.K. Nazeeruddin, T. Torres, Phthalocyanines for dye-sentisized solar cells, Coord. Chem. Rev. 381 (2019) 1.
[4] A.B. Sorokin, Phthalocyanine metal complexes in catalysis, Chem. Rev. 113 (2013) 8152.
[5] E. Yabaş, E. Biçer, R. Katırcı, Experimental and in silico studies on optical properties of new thiadiazole tetrasubstituted metal-free and zinc phthalocyanine compounds, Opt. Mater. (2021), doi:10.1016/j.optmat.2021.111808.
[6] C.G. Claessens, U. Hahn, T. Torres, Phthalocyanines: from outstanding electronic properties to emerging applications, Chem. Rec. 8 (2008) 75.
[7] R. Ramachandran, Q. Hu, K. Rajavel, P. Zhu, C. Zhao, F. Wang, Z.X. Xu, Non-peripheral octamethyl-substituted copper (II) phthalocyanine nanorods with MXene sheets: An excellent electrode material for symmetric supercapacitor with enhanced electrochemical performance, J. Power Sources 471 (2020) 228472.
[8] M. Samanta, P. Howli, U.K. Ghorai, M. Mukherjee, C. Bose, K.K. Chattopadhyay, Solution processed copper phthalocyanine nanowires: a promising supercapacitor anode material, Phys. E 114 (2019) 113654.
[9] T. Chen, L. Dai, Carbon nanomaterials for high-performance supercapacitors, Mater. Today 16 (2013) 272.
[10] M.I.A. Abdel Maksoud, R.A. Fahim, A.E. Shalan, M.A. Elkodous, S.O. Olojede, A.I. Osman, C. Farrell, A.H. Al–Muhtaseb, A.S. Awed, A.H. Ashour, D.W. Rooney, Advanced materials and technologies for supercapacitors used in energy conversion and storage: a review, Environ. Chem. Lett. 19 (2021) 375.
[11] K.P. Madhuri, N.S. John, Supercapacitor application of nickel phthalocyanine nanofibres and its composite with reduced graphene oxide, Appl. Surf. Sci. 449 (2018) 528.
[12] S. Pillay, J. Pillay, P.M. Ejikeme, K. Makgopa, K.I. Ozoemena, Nanostructured cobalt(II) tetracarboxyphthalocyanine complex supported within the MWCNT frameworks: electron transport and charge storage capabilities, Electroanal 27 (2015) 1707.
[13] L. Mei, X. Cui, Q. Duan, Y. Li, X. Lv, H.G. Wang, Metal phthalocyanine-linked conjugatedmicroporous polymer hybridized with carbonnanotubes as a high--performance flexible electrodefor supercapacitors, Int. J. Hydrog. Energy 45 (2020) 22950.
[14] O. Gorduk, M. Gencten, S. Gorduk, M. Sahin, Y. Sahin, Electrochemical fabrication and supercapacitor performances of metallo phthalocya-

nine/functionalized-multiwalled carbon nanotube/polyaniline modified hybrid electrode materials, J. Energy Storage 33 (2021) 102049.
[15] L. Yang, K. Zhuo, X. Xu, Z. Zhang, Q. Du, Y. Chen, D. Sun, J. Wang, Redox-active phthalocyanine-decorated graphene aerogels for high-performance supercapacitors based on ionic liquid electrolyte, J. Mater. Chem. A 8 (2020) 21789.
[16] Z. Xu, G. Zhang, Z. Cao, J. Zhao, H. Li, Effect of N atoms in the backbone of metal phthalocyanine derivatives on their catalytic activity to lithium battery, J. Mol. Catal. A Chem. 318 (2010) 101.
[17] F. Ghani, J. Kristen, H. Riegler, Solubility properties of unsubstituted metal phthalocyaninesin different types of solvents, J. Chem. Eng. Data 57 (2012) 439.
[18] Q. Ke, J. Wang, Graphene-based materials for supercapacitor electrodes - a review, J. Mater. 2 (1) (2016) 37–54.
[19] A. Bakandritsos, D.D. Chronopoulos, P. Jakubec, M. Pykal, K. Čépe, T. Steriotis, S. Kalytchuk, M. Petr, R. Zbořil, M. Otyepka, High-performance supercapacitors based on a zwitterionic network of covalently functionalized graphene with iron tetraaminophthalocyanine, Adv. Funct. Mater. 28 (2018) 1801111.
[20] W.L.F. Armarego, C.L.L. Chai, Purification of Laboratory Chemicals, Butterworth/Heinemann, Elsevier, Tokyo, 2003.
[21] E. Bağda, E. Yabaş, E. Bağda, Analytical approaches for clarification of DNA–double decker phthalocyanine binding mechanism: as an alternative anticancer chemotherapeutic, Spectrochim. Acta A Mol. Biomol. Spectros. 172 (2017) 199.
[22] G. Gümrükçü, M. Üstün-Özgür, A. Altındal, A.R. Özkaya, B. Salih, Ö. Bekaroğlu, Synthesis and electrochemical, electrical and gas sensing properties of novel mononuclear metal-free, Zn(II), Ni(II), Co(II), Cu(II), Lu(III) and double-decker Lu(III) phthalocyanines substituted with 2-(2H-1,2,3-benzotriazol-2-yl)-4-(1,1,3,3-tetramethylbutyl)phenoxy, Synth. Met. 161 (2011) 112.
[23] E. Yabaş, M. Sülü, F. Dumludağ, A.R. Özkaya, B. Salih, Ö. Bekaroğlu, Electrical and electrochemical properties of double-decker Lu(III) and Eu(III) phthalocyanines with four imidazoles and N-alkylated imidazoles, Polyhedron 42 (2012) 196.
[24] E. Yabaş, New cobalt phthalocyanine–graphene oxide hybrid nanomaterial prepared by strong π–π interactions, J. Aust. Ceram. Soc. (2021).
[25] X.F. Zhang, X. Shao, π-π-Binding ability of different carbon nano-materials with aromatic phthalocyanine molecules: comparison between graphene, graphene oxide and carbon nanotubes, J. Photochem. Photobiol. A 278 (2014) 69.
[26] P. Das, K. Chakraborty, S. Chakrabarty, S. Ghosh, T. Pal, Reduced graphene oxide - zinc phthalocyanine composites as fascinating material for optoelectronic and photocatalytic applications, ChemistrySelect 2 (2017) 3297.
[27] I.S. Hosu, Q. Wang, A. Vasilescu, S.F. Peteu, V. Raditoiu, S. Railian, V. Zaitsev, K. Turcheniuk, Q. Wang, M. Li, R. Boukherroub, S. Szunerits, Cobalt phthalocyanine tetracarboxylic acid modified reduced graphene oxide: a sensitive matrix for the electrocatalytic detection of peroxynitrite and hydrogen peroxide, RSC Adv. 5 (2015) 1474–1484.
[28] P. Aryanrad, H.R. Nader, E. Kohan, M.R. Ganjali, M. Baghernejad, S. Dezfuli, Europium oxide nanorod-reduced graphene oxide nanocomposites towards supercapacitors, RSC Adv. 10 (2020) 17543.
[29] A. Lasia, The origin of the constant phase element, J. Phys. Chem. Lett. 13 (2022) (2022) 580–589.
[30] C. Yun, S. Hwang, Analysis of the charging current in cyclic voltammetry and supercapacitor's galvanostatic charging profile based on a constant-phase element, ACS Omega 6 (2021) 367–373.
[31] E. Cuervo-Reyes, C.P. Scheller, M. Held, U. Sennhauser, A unifying view of the constant-phase-element and its role as an aging indicator for Li-ion batteries, J. Electrochem. Soc. 162 (2015) A1585–A1591.